

Computational Fluid Dynamics Study of Compact Methanol Steam Reformer for Aviation Applications

Haoyu Du¹, Zhaohuan Zhang¹, Kai Xv², Xiaoqing Zhang², Xiao Ma¹, Shijin Shuai^{1,2}

¹State Key Laboratory of Intelligent Green Vehicle and Mobility, School of Vehicle and Mobility, Tsinghua University, Beijing, 100084, China; ²Institute for Aero Engine, Tsinghua University, Beijing, 100084, China

National Key Research & Development Program of China (Grant Number 2021YFB2500400)

Abstract: In this study, a computational fluid dynamics (CFD) study focused on a compact methanol steam reaction (MSR) reformer for aviation applications is proposed. Three-dimensional (3-D) transient CFD models of 1 kW MSR reformers are developed to analyze the start-up period, optimize geometric configurations and flow modes. The effect of heating tube position, heating film position, reformer diameter and length are studied. And counter-flow is found to be the more suitable choice than co-flow. Strategies are proposed to enhance methanol conversion rates and accelerate start-up phase to improve the reliability and compactness of reformers in aviation power systems.

Keywords: Computational Fluid Dynamics; Methanol Steam Reformer; Aviation Power System; Geometric Configuration Optimization

1 Introduction

In the aviation field, the reformer plays a critical role by enhancing the fuel flexibility of power systems. It is utilized to catalyze aviation fuels such as petroleum products or biomass fuels into hydrogen and carbon monoxide, which can be used in gas turbine (GT) systems. Additionally, the aviation industry faces new demands for power systems due to the growing pressure to reduce fuel consumption, pollutants, and noise emissions. Consequently, there is a significant drive to apply fuel cells as aircraft auxiliary power units (APUs) [1]. For the reliability and durability of fuel cells, the reformer is required in the proton exchange membrane fuel cell (PEMFC) or solid oxide fuel cell (SOFC) system.

The Aviation Application demands high reliability and integration for reformers. Therefore, studies of internal multi-physics fields and feasible geometric optimization are necessary. Besides, the dynamic response of reformers, such as the start-up speed, also requires attention. Experimental research related to reformers mainly focuses on the development of catalyst materials [2-4]. However, considering cost constraints, numerical studies are more prevalent. Liu et al. [5] developed a model of SOFC - GT hybrid system for electric propulsion aircraft with reforming process model to investigate the effect of fuel types. Similar 0-D or 1-D system modeling studies focus on the input and output parameters of reformers, without considering internal states and structural design. Therefore, the multi-dimensional modeling approach for reformers is important. Peksen et al. [6] introduced a 3-D computational fluid dynamics (CFD) model of a methane steam reformer, which was validated using experimental data. Klenov et al. [7] proposed a novel configuration of a compact methanol processor

integrated with a methanol steam reformer, a catalytic combustor, and a fuel evaporator, establishing a steady model to validate the design feasibility. Wismann et al.^[8] utilized a 2-D transient model to estimate carbon deposition in a methane steam reformer and investigated the cold start and transient response. At present, research on reformer models developed for aviation applications, especially multi-dimensional transient models, is relatively scarce.

Regarding fuel selection, methanol stands out as a favorable option due to its high volumetric energy density, easy transportation and storage, and low level of impurities^[9, 10]. Moreover, methanol is a clear and renewable source which can be produced from agricultural byproducts and biomass fermentation or gasification^[11]. One of the most commonly applied reforming reactions in external reformers is the methanol steam reforming (MSR) reaction, with a reaction temperature range of 493 – 573 K^[4, 12].

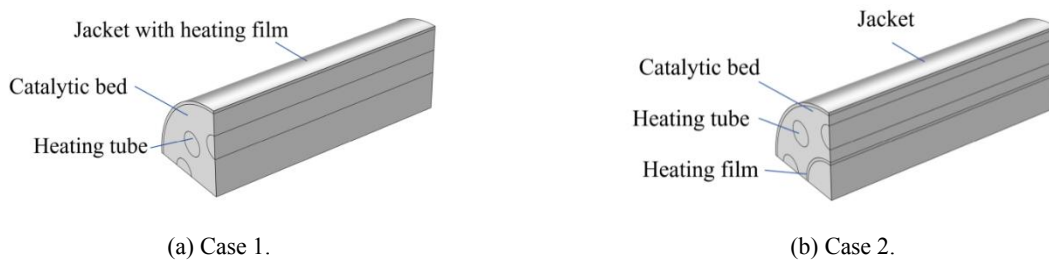
In this paper, 3-D CFD transient models for a 1 kW MSR reformer were constructed, and the start-up period of the reformer was analyzed based on the model. Geometric configuration optimization and flow mode selection for the reformer were also implemented. Finally, strategies to improve methanol conversion rate and accelerate start-up rate were proposed and reasons were analyzed, benefiting the reliability and compactness of reformers in aviation power systems.

2 Numerical Model

2.1 Computational domain and assumptions

In this study, three new configurations based on the conventional 1 kW MSR reformer geometry are proposed, and the start-up process is investigated using a 3-D CFD transient model. During the start-up period, the temperature of the reformer should be rapidly heated from 373 K to its operating temperature. To reduce computational costs, 1/4 of the reformers are selected as the computational domain, as shown in Fig.1. Case 1 shows the conventional reformer which consists of three parts: a jacket with the heating film, a catalytic bed, and heating tubes using waste heat from exhaust gas. The position of the heating film is adjusted in cases 2 and 3, while the diameter and length of the reformer are altered in case 4. Geometric parameters of four cases are shown in Table 1. In all four cases, the volume, temperature, inlet flow rate, and other conditions of the reformer are kept identical, as shown in Table 2, and the catalyst used is the commercial Cu/ZnO/Al₂O₃ material. The simulation was conducted to analyze the transient responses in the multi-physical fields of the reformer 600 seconds after the introduction of the fuel gas, and a time step of 2 seconds was used. Furthermore, the reformer model is based on the following assumptions.

1. All the gas species are ideal gases;
2. The flow is laminar;
3. The effects of body forces and gravity are ignored;
4. The catalytic bed is considered to be isotropic and homogeneous, and reactions of chemical species take place only in the catalytic bed.



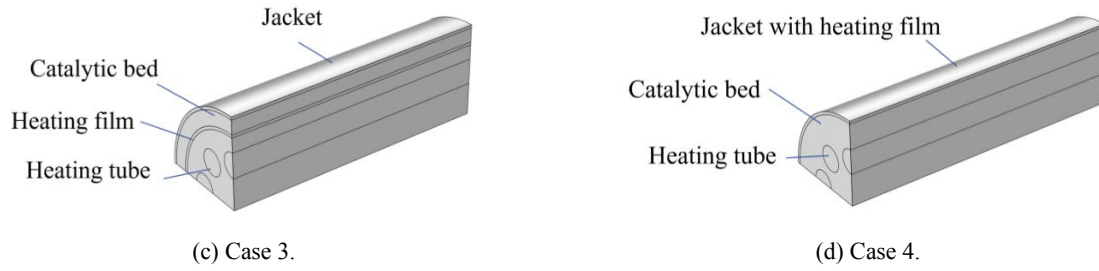


Fig.1 Computational domain of reformer models.

Table 1 Geometric parameters.

Parameters	Symbol	Value			
		Case 1	Case 2	Case 3	Case 4
Length (mm)	L	180	180	180	200
Diameter of reformer (mm)	D_R	128	128	128	122
Diameter of catalytic bed (mm)	D_C	124	124	124	118
Diameter of heating tube (mm)	d_h	17.6	17.6	17.6	17.6
Distance from the center of the heating tube to the center of the reformer (mm)	l_1	31/34/37	46	31	32
Distance from the center of the heating film to the center of the reformer (mm)	l_2	124	56	100	118

Table 2 Operating parameters.

Parameters	Symbol	Value
Operating pressure (atm)	P	1
Ambient temperature (K)	T_{amb}	373
Inlet temperature of the reformer (K)	T_{in}	373
Inlet space velocity (h^{-1})	SV_0	290
Inlet molar flow rate of methanol (mmol/s)	n	2.1
Inlet steam-to-carbon ratio	SCR	1.5
Inlet temperature of heating tubes (K)	T_h	673
Inlet velocity of heating tubes ($m\ s^{-1}$)	v_h	1
Heating film power (W)	P	110

2.2 Multi-physical fields modeling

The gas flow in the reformer model is divided into two types: porous medium flow in the catalytic bed and laminar flow in heating tubes. Mass, momentum, and energy conservation equations are established for both sections of the flow. As for the chemical kinetic modeling, two major reactions are considered which are MSR reaction and water gas shift (WGS) reaction^[13]. The Arrhenius model is utilized to assess the rates of chemical reactions. Table 3 and 4 shows the multi-physical fields modeling equations and parameters in the numerical model.

Table 3 Multi-physical model.

Model	Equation
Mass conservation of porous medium flow	$\frac{\partial}{\partial t}(\rho\omega_i) + \nabla \cdot (\rho\omega_i \mathbf{u}) + \nabla \cdot \mathbf{j}_i = R_i$
Momentum conservation of porous medium flow	$\mathbf{j}_i = -\rho\omega_i \sum_{k=1}^n \tilde{D}_{ik} (\nabla y_k + (y_k - \omega_k) \frac{\nabla p}{p}) - D_i^T \frac{\nabla T}{T}$
Energy conservation of porous medium flow	$\frac{\partial(\varepsilon\rho)}{\partial t} + \nabla \cdot (\rho\mathbf{u}) = Q_m$
Energy conservation of porous medium flow	$(\rho C_p)_{\text{eff}} \frac{\partial T}{\partial t} + \rho C_{p,g} \mathbf{u} \cdot \nabla T + \nabla \cdot (-k_{\text{eff}} \nabla T) = Q$
Mass conservation of laminar flow	$\rho \frac{\partial \mathbf{u}}{\partial t} = -\nabla p + \nabla \cdot [\mu(\nabla \mathbf{u} + (\nabla \mathbf{u})^T)] - \frac{2}{3} \mu(\nabla \cdot \mathbf{u}) \mathbf{I}$
Momentum conservation of laminar flow	$\frac{\partial \rho}{\partial t} + \nabla \cdot (\rho\mathbf{u}) = 0$
Energy conservation of laminar flow	$\rho_g C_{p,g} \frac{\partial T}{\partial t} + \rho_g C_{p,g} \mathbf{u} \cdot \nabla T + \nabla \cdot (-k_g \nabla T) = 0$
Rate of MSR reaction	$R_{\text{MSR}} = k_1 C_{\text{CH}_3\text{OH}}^{0.6} C_{\text{H}_2\text{O}}^{0.4} \exp\left(-\frac{E_{a1}}{RT}\right)$
Rate of reverse WGS reaction	$R_{\text{rWGS}} = k_2 C_{\text{CO}_2} C_{\text{H}_2} \exp\left(-\frac{E_{a2}}{RT}\right) - k_{-2} C_{\text{CO}} C_{\text{H}_2\text{O}} \exp\left(-\frac{E_{a-2}}{RT}\right)$

Table 4 Parameters in the reformer model.

Parameters	Symbol	Value
Heat transfer coefficient of heating tube ($\text{W m}^{-2} \text{K}^{-1}$)	h_h	100
Density of catalytic bed (kg m^{-3}) ^[14]	ρ_c	1480
Specific heat capacity of catalytic bed ($\text{J kg}^{-1} \text{K}^{-1}$)	$C_{p,c}$	400
Thermal conductivity of catalytic bed ($\text{W m}^{-1} \text{K}^{-1}$)	λ_c	1
Catalytic bed porosity ^[14]	ε	0.5
Permeability of catalytic bed (m^2) ^[14]	κ	2.379×10^{-12}
Density of jacket (kg m^{-3})	ρ_j	24
Specific heat capacity of the jacket ($\text{J kg}^{-1} \text{K}^{-1}$)	$C_{p,j}$	19
Thermal conductivity of jacket ($\text{W m}^{-1} \text{K}^{-1}$)	λ_j	0.027
Universal gas constant ($\text{J mol}^{-1} \text{K}^{-1}$)	R	8314
Pre-exponential factor for MSR (s^{-1}) ^[15, 16]	k_1	8×10^8
Pre-exponential factor for reverse WGS ($\text{m}^3 \text{mol}^{-1} \text{s}^{-1}$) ^[15, 16]	k_2	4×10^8
Pre-exponential factor for backward WGS ($\text{m}^3 \text{mol}^{-1} \text{s}^{-1}$) ^[15, 16]	k_{-2}	4×10^8
Activation energy for MSR (J mol^{-1}) ^[15, 16]	E_{a1}	7×10^7
Activation energy for reverse WGS (J mol^{-1}) ^[15, 16]	E_{a2}	1×10^8
Activation energy for backward WGS (J mol^{-1}) ^[15, 16]	E_{a-2}	1×10^8

2.3 Numerical procedure

The 3-D numerical reformer model were discretized using the finite volume method (FVM). The commercial CFD software COMSOL MULTIPHYSICS 6.0 was employed for conducting the numerical study.

Integrated modules within COMSOL, such as Chemistry, Darcy's Law, Transport of Concentrated Species, and Heat Transfer in Porous Media, were utilized to analyze chemical reaction kinetics, fluid heat, and mass transfer. The implicit time-stepping method BDF was applied to solve time-dependent problems, with the convergence criteria set for all residual values to be less than 10^{-5} .

2.4 Grid independence study and model validation

Grid independence was assessed through a series of tests for different cases. A structured mesh with a boundary layer mesh structure was adopted. For case 1, the average outlet H_2 and CO molar concentration at 600 s for various grid sizes are shown in Fig.2. It was noted that when the grid size reached 61,696, both the average outlet H_2 and CO molar concentration values became relatively stable. As a result, to optimize computational efficiency and ensure accurate results, a grid size of 61,696 was chosen for the numerical study. For other cases, the same meshing method was employed, and the corresponding grid sizes were determined.

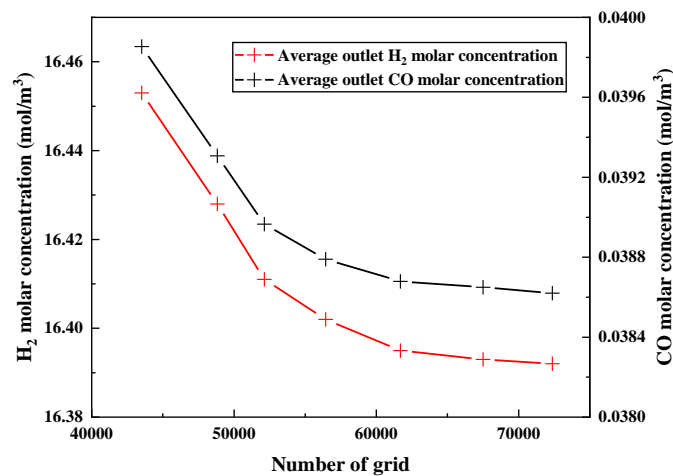


Fig.2 Grid independence study of case 1.

To verify the accuracy of the numerical model, this paper compares the simulation results of case 1 at 600 s with the experimental data by Yang et al.^[17] as shown in Fig.3. The heating temperature of the reformer was 1000 K, and SCR was 1.5 and 2.0 respectively. The simulated component molar fraction closely matched the experimental data, which confirms the reliability of using CFD models for further investigations.

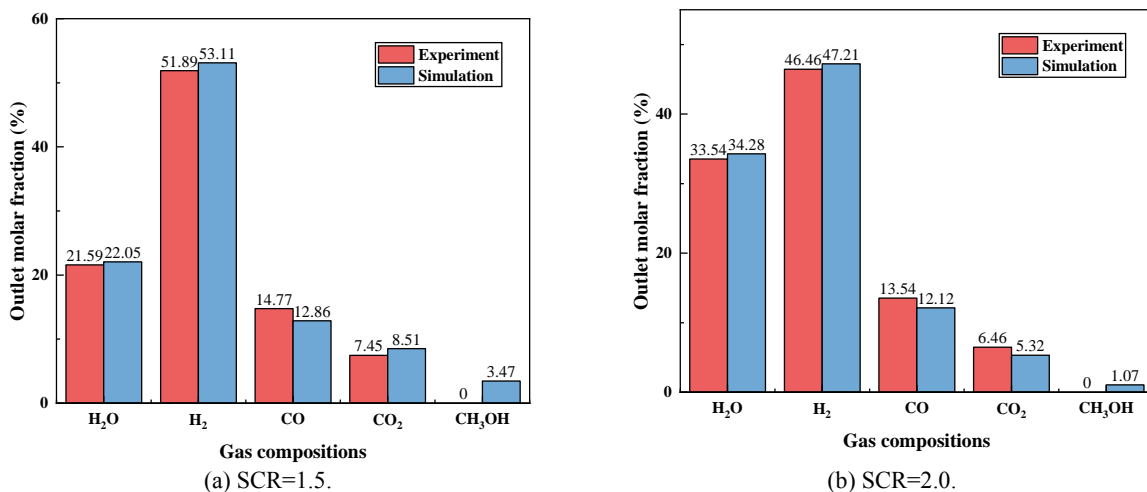


Fig.3 Comparison with experimental data^[17].

3 Results and discussions

3.1 Start-up period of MSR reformer

The 3-D CFD transient model established in this work enables a better understanding of the multi-physical fields during the start-up process of the MSR reformer. The changes of H₂ molar concentration and temperature field of case 1, conventional reformer, are shown in Fig.4. During the start-up process, the temperature of the reformer continuously increase due to heat transfer from the heating film and heating tubes, leads to an increase in the quantity of H₂. Regions near the heating film and heating tubes exhibit higher temperatures, and the end of the reformer reaches higher temperatures, making it a design area where thermal constraints need to be considered. The maximum H₂ molar concentration and total H₂ production increase over time. However, in the end region of the reformer, the high temperature results in a higher reforming endothermic reaction rate and significant gas mass transfer effects, leading to a lower H₂ molar concentration. According to the simulation results, the start-up process of the reformer lasts for 400 s, and after then it enters a steady state.

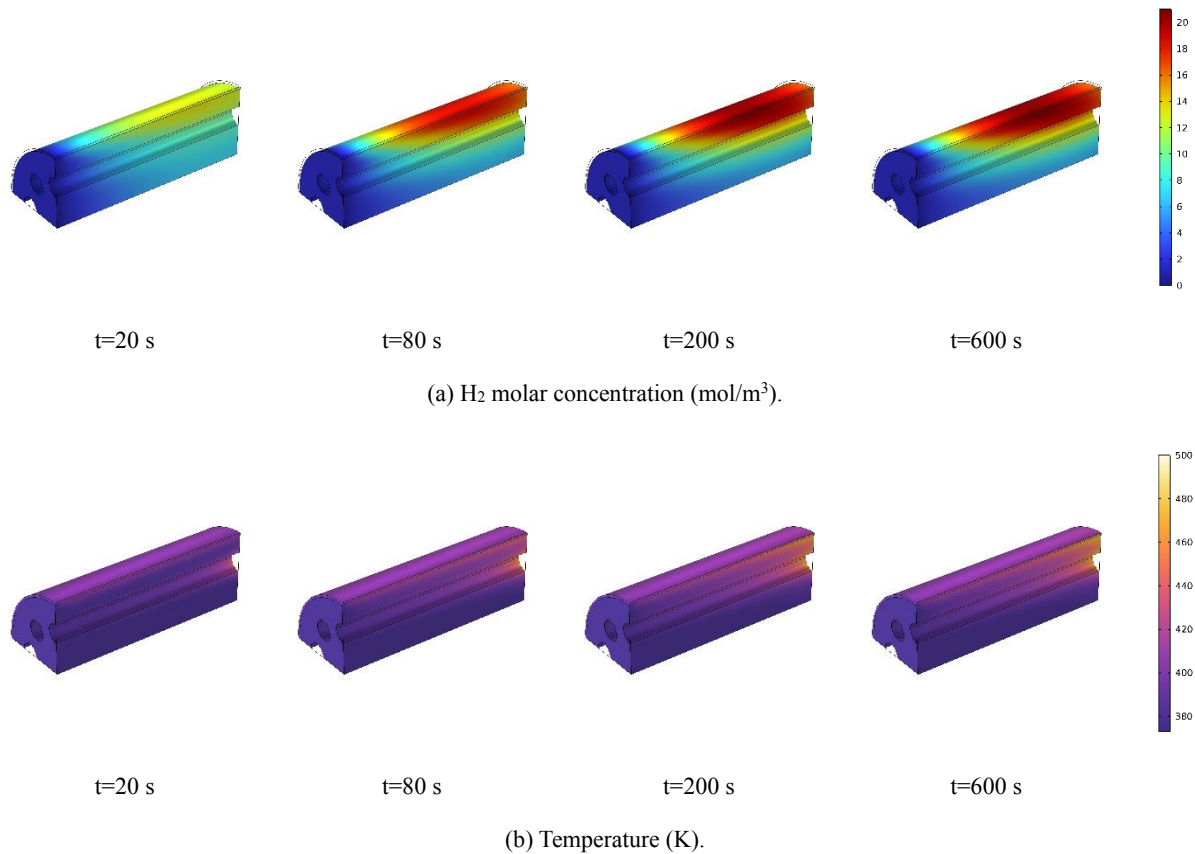


Fig.4 Start-up period of case 1.

3.2 Geometric configuration optimization

For Aviation Applications, issues of volume and compactness need to be considered. To enhance reforming efficiency within limited space, geometric optimization is necessary. Through simulation, the effect of heating tube position, heating film position, reformer diameter and length have been studied, providing guidance for compacting the structure of reformers in aviation power systems.

3.2.1 Effect of heating tube position

The position of the heating tubes has an impact on the internal heat transfer of the reformer. In case 1, the

distance from the center of the heating tube to the center of the reformer was simulated at 31 mm, 34 mm, and 37 mm, respectively. Results of these three models in which H₂ molar fraction and methanol conversion are compared, are shown in Fig.5. When the heating tube is positioned 34 mm away from the center of the reformer, the H₂ molar fraction and methanol conversion show the highest rate of increase during the start-up, and values are also highest after reaching stability. This could be due to the optimal distance between the heating tube and heating film, resulting in a higher overall temperature inside the reformer and a smaller low-temperature region, leading to a faster reforming reaction rate. When the distance is 31 mm, the performance of the reformer is the least desirable.

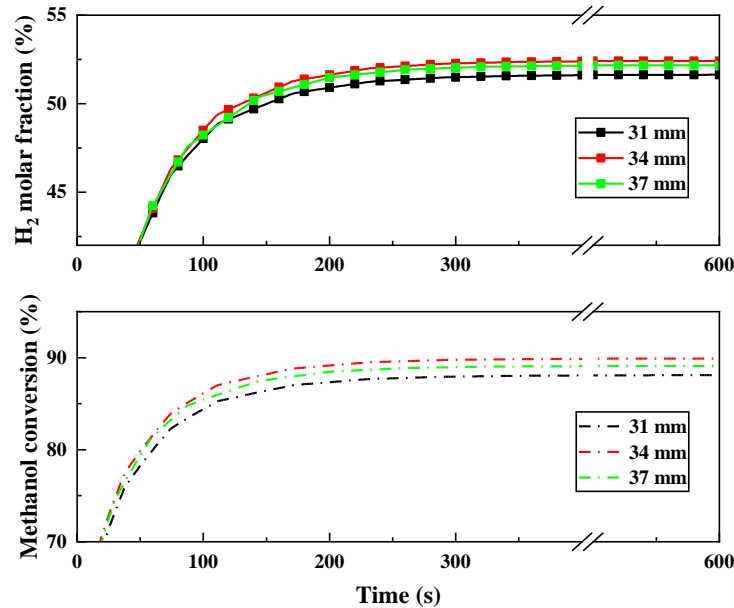


Fig.5 Effect of heating tube position.

3.2.2 Effect of heating film position

In the conventional configuration, the heating film is placed inside the jacket, resulting in significant heat loss to the external environment. Therefore, this study considered the effect of changing the position of the heating film, and cases 1-3 were simulated. In case 1, the distance from the center of the heating tube to the center of the reformer is 34 mm. The change of the position of the heating film results in increased start-up speed and reduced start-up time, attributed to the decrease in heat transfer losses. The arrangement of the heating film in case 2 corresponded to the highest start-up speed. When the reformer reached a steady state, both the H₂ molar fraction and methanol conversion in case 1 and 2 are greater than those in case 3, especially methanol conversion showing an increase of approximately 4%. This indicates that an optimal position for the heating film can enhance the fuel reforming efficiency. To further explain the reasons of difference, the start-up period of case 2 is shown in Fig.7. Compared with case 1, the trend of changes of H₂ molar concentration and temperature field in case 2 is similar, with consistent patterns of high temperature and high H₂ concentration regions. However, due to reduced heat transfer losses, the region near the heating film at the rear of the reformer becomes a high-temperature zone in case 2, with temperatures higher than case 1. As a result, the area with high H₂ production is larger, and the maximum production is also greater. Therefore, placing the heating film inside the reformer is advantageous for rapid start-up and hydrogen generation. In the same volume, although increasing costs, there is a possibility of better performance for case 2 and 3.

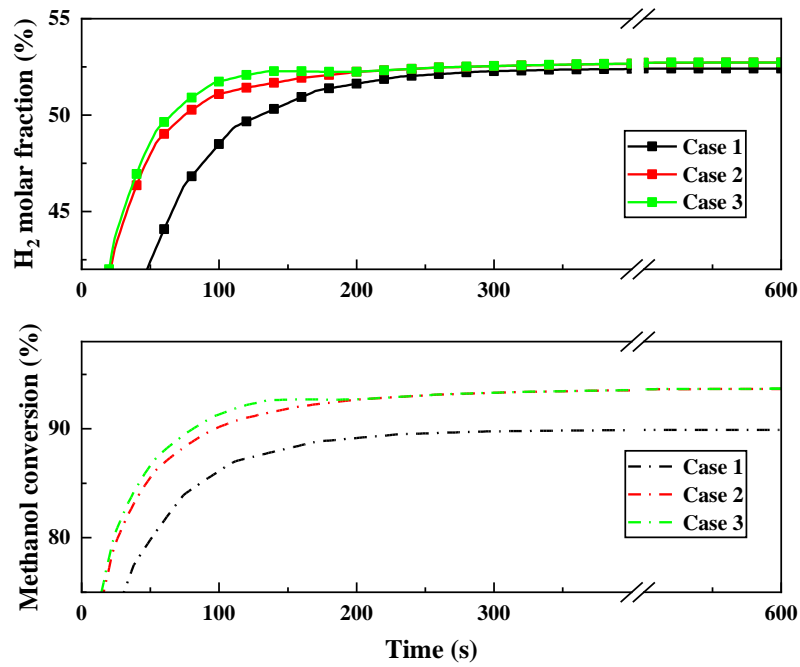


Fig.6 Effect of heating film position.

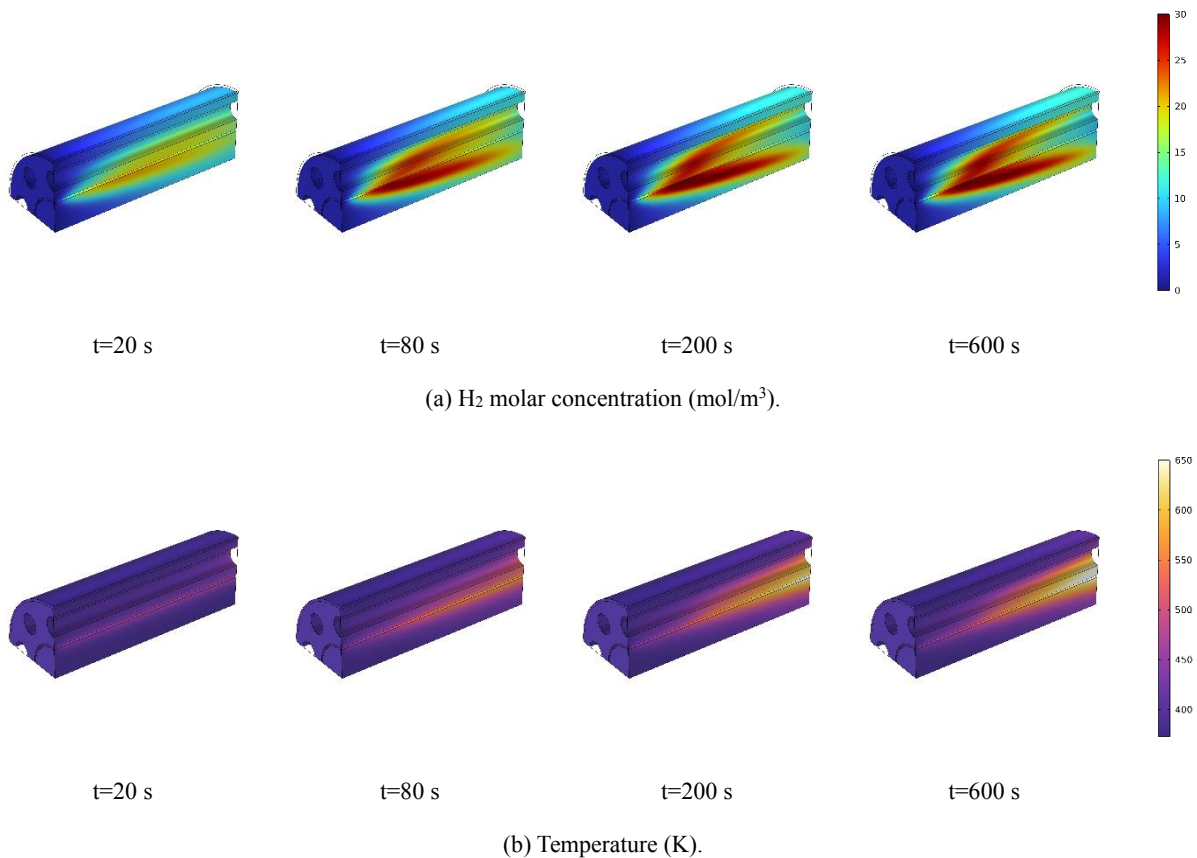


Fig.7 Start-up period of case 2.

3.2.3 Effect of diameter and length of reformer

In aviation power systems, space is limited. Additionally, for system integration purposes, different systems may have different requirements for the shape of the reformer. To investigate the impact of geometric parameters

such as diameter and length on the performance of the reformer under the condition of equal volume, a comparison was made between the results of case 1 and case 4, as shown in Fig.8. In case 4, the diameter of the reformer is reduced while the length is increased, resulting in a smaller distance between the heating tube and heating film. Consequently, there is a concentration of heat and a larger high-temperature region, leading to better performance than case 1. In practical applications, if the system space allows, it is advisable to increase the length and decrease the diameter accordingly.

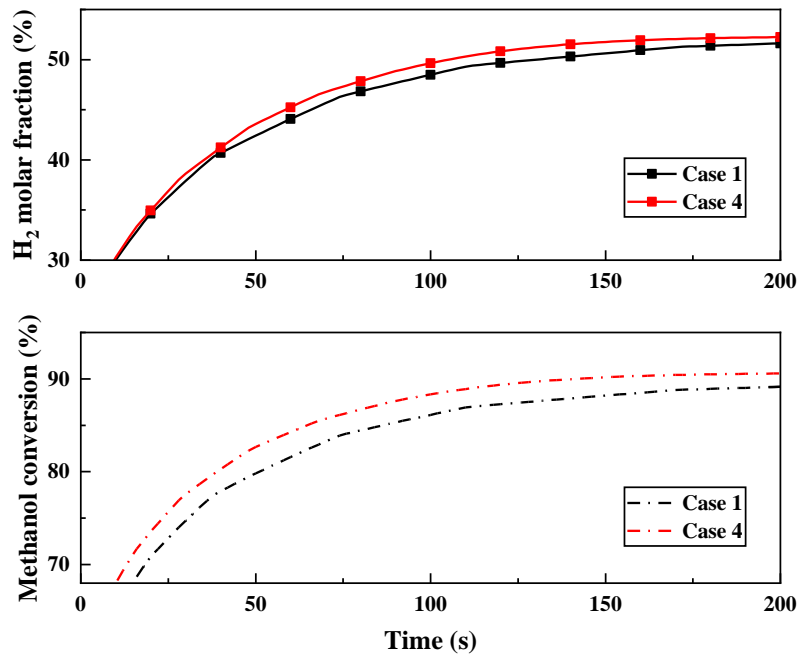


Fig.8 Effect of heating geometric parameters.

3.3 Impact of gas flow mode

The direction of gas flow in heating tubes, whether it is counter-flow or co-flow with the reactant gas, can significantly influence the performance of the reformer, especially affecting heat transfer during the start-up phase. Counter-flow and co-flow refer to gas flow modes where the two gas flows have opposite or the same directions respectively. Therefore, the flow mode needs to be carefully considered in the design and optimization of the reformer. The impact of gas flow modes on outlet parameter results is shown in Fig.9, and the counter-flow mode shows better performance for both cases. Cross-sectional plots of the temperature fields are shown in Fig.10 to explain the reasons for the different results of various gas flow modes. Five equidistant cross-sections along the x-axis were cut to divide the reformer into six evenly spaced parts for case 2. For the counter-flow mode, due to the higher temperature at the inlet of the heating tube, a larger high-temperature region is formed at the end of the reformer under the combined effect of the heating tube inlet and the heating film; while for the co-flow mode, the high-temperature region at the end of the reformer is smaller and the temperature is lower. However, the low-temperature region is smaller and the temperature is higher near the inlet of the heating tube at the front of the reformer. Therefore, it can be inferred that expanding the specific area and increasing the temperature of the high-temperature region with concentrated heat are more favorable for reformer start-up and methanol conversion than raising the temperature in the low-temperature region. This insight provides guidance for the design of reducing the size of the reformer and improving its performance in aviation power systems.

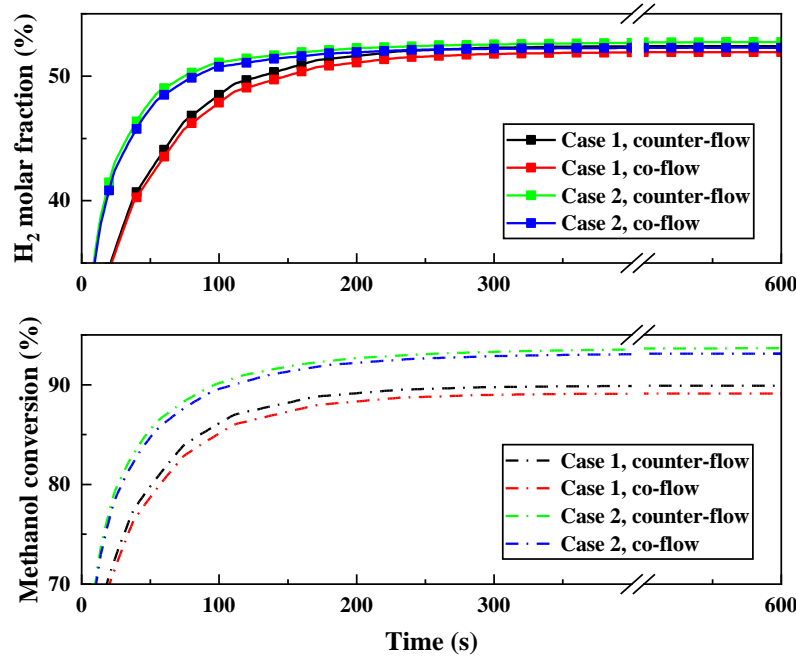


Fig.9 Effect of gas flow mode.

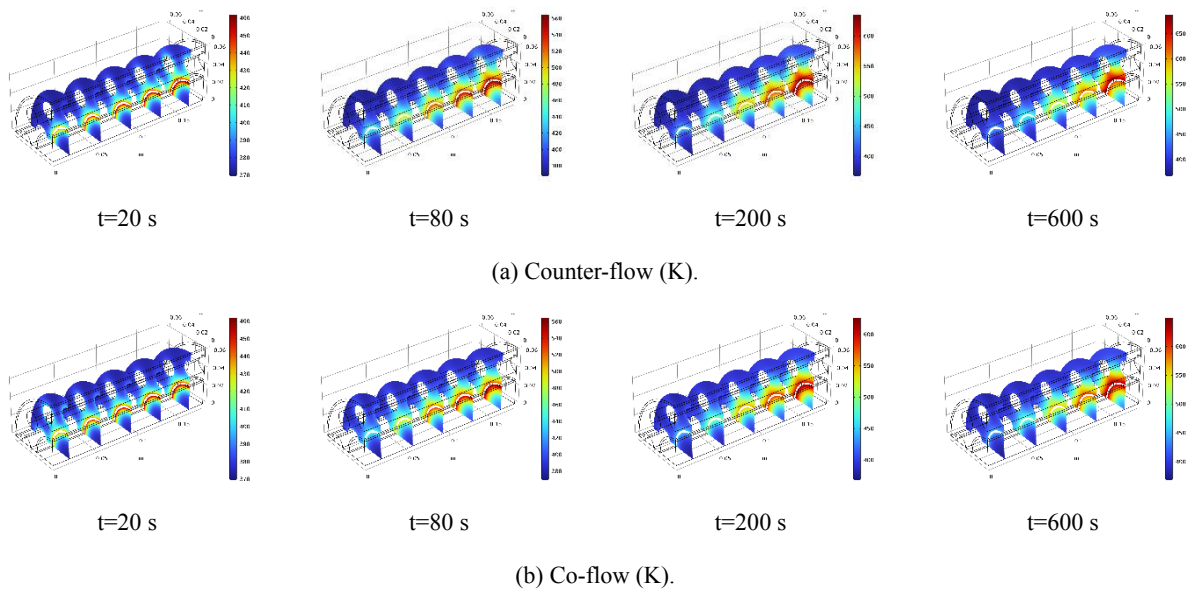


Fig. 10 Cross-sectional temperature field of different gas flow modes of case 2.

4 Conclusion

This work proposes 3-D CFD transient models of 1 kW MSR reformers. Based on the reformer model, the start-up performance and feasible geometric configuration optimization are analyzed. The main conclusions of the present study are summed up as follows:

- (1) By establishing 3-D transient models, the start-up process of conventional MSR reformer was studied. The multi-physical field changes inside the reformer have been investigated.
- (2) Considering the space limitations and reliability requirements of aviation systems, optimization was conducted on the geometric configuration of the reformer, including the position of the heating tube and heating film, as well as the diameter and length of the reformer. This optimization process provides a reference for compacting the design of reformers in aviation systems.

(3) Counter-flow was found to be the more suitable gas flow mode in MSR reformer. By analyzing the temperature field and heat transfer inside the reformer, it was suggested that increasing the volume or temperature of the high-temperature zone is more favorable for reformer start-up than raising the temperature of the low-temperature zone, which could be considered as one of the guidelines for future MSR reformer design for aviation applications.

Reference:

- [1] FERNANDES M D, S D P ANDRADE, V N BISTRITZKI, 等. SOFC-APU systems for aircraft: A review [J]. 2018, 43(33): 16311-33.
- [2] YONG S T, C W OOI, S-P CHAI, 等. Review of methanol reforming-Cu-based catalysts, surface reaction mechanisms, and reaction schemes [J]. 2013, 38(22): 9541-52.
- [3] Sá S, H SILVA, L BRANDÃO, 等. Catalysts for methanol steam reforming—A review [J]. 2010, 99(1-2): 43-57.
- [4] HERDEM M S, M Y SINAKI, S FARHAD, 等. An overview of the methanol reforming process: Comparison of fuels, catalysts, reformers, and systems [J]. 2019, 43(10): 5076-105.
- [5] LIU H, J QIN, X XIU, 等. Comparative study of fuel types on solid oxide fuel cell - gas turbine hybrid system for electric propulsion aircraft [J]. 2023, 347: 128426.
- [6] PEKSEN M, R PETERS, L BLUM, 等. Numerical modelling and experimental validation of a planar type pre-reformer in SOFC technology [J]. 2009, 34(15): 6425-36.
- [7] KLENOV O, L MAKARSHIN, A GRIBOVSKIY, 等. CFD modeling of compact methanol reformer [J]. 2015, 282: 91-100.
- [8] WISMANN S T, J S ENGBAEK, S B VENDELBO, 等. Electrified methane reforming: Elucidating transient phenomena [J]. 2021, 425: 131509.
- [9] CIMENTI M, V ALZATE-RESTREPO, J M J J O P S HILL. Direct utilization of methanol on impregnated Ni/YSZ and Ni - ZrO. 35Ce0. 65O2/YSZ anodes for solid oxide fuel cells [J]. 2010, 195(13): 4002-12.
- [10] LIU M, R PENG, D DONG, 等. Direct liquid methanol-fueled solid oxide fuel cell [J]. 2008, 185(1): 188-92.
- [11] JIANG Y, A V J J O T E S VIRKAR. A high performance, anode-supported solid oxide fuel cell operating on direct alcohol [J]. 2001, 148(7): A706.
- [12] AGARWAL V, S PATEL, K J A C A G PANT. H₂ production by steam reforming of methanol over Cu/ZnO/Al₂O₃ catalysts: transient deactivation kinetics modeling [J]. 2005, 279(1-2): 155-64.
- [13] PURNAMA H, T RESSLER, R E JENTOFT, 等. CO formation/selectivity for steam reforming of methanol with a commercial CuO/ZnO/Al₂O₃ catalyst [J]. 2004, 259(1): 83-94.
- [14] KARIM A, J BRAVO, A J A C A G DATYE. Nonisothermality in packed bed reactors for steam reforming of methanol [J]. 2005, 282(1-2): 101-9.
- [15] AGRELL J, H BIRGERSSON, M J J O P S BOUTONNET. Steam reforming of methanol over a Cu/ZnO/Al₂O₃ catalyst: a kinetic analysis and strategies for suppression of CO formation [J]. 2002, 106(1-2): 249-57.
- [16] FUKAHORI S, H KOGA, T KITAOKA, 等. Steam reforming behavior of methanol using paper-structured catalysts: experimental and computational fluid dynamic analysis [J]. 2008, 33(6): 1661-70.
- [17] YANG B, Y LIU, J ZHU, 等. The Performance of Solid Oxide Fuel Cells Based on Methanol Solution [J]. 2023, 111(6): 1575.